

Very high contrast IFU spectroscopy of AB Doradus C: 9 mag contrast at $0''.2$ without a coronagraph using spectral deconvolution. ^{*}

Niranjan Thatte¹, Roberto Abuter², Matthias Tecza¹, Eric L. Nielsen³,
Fraser J. Clarke¹, & Laird M. Close³

¹ Department of Astrophysics, Denys Wilkinson Building, Keble Road, Oxford, OX1 3RH.

² Max-Planck-Institut für extraterrestrische Physik & European Southern Observatory, D-85748, Garching, Germany.

³ Steward Observatory, University of Arizona, Tucson, AZ 85721, U.S.A.

email: nthatte@astro.ox.ac.uk (NT), rabuter@eso.org (RA), mtezza@astro.ox.ac.uk (MT), enielsen@as.arizona.edu (EN),
fclarke@astro.ox.ac.uk (FJC), lclose@as.arizona.edu (LMC)

accepted 2007 March 8, received 2007 March 8, in original form 2006 June 6

ABSTRACT

We present an extension of the spectral deconvolution method (Sparks & Ford 2002) to achieve very high contrast at small inner working radii. We apply the method to the specific case of ground based adaptive optics fed integral field spectroscopy (without a coronagraph). Utilising the wavelength dependence of the Airy and speckle patterns, we make an accurate estimate of the PSF that can be scaled and subtracted from the data cube. The residual noise in the resulting spectra is very close to the photon noise from the starlight halo. We utilise the technique to extract a very high SNR H & K band spectrum of AB Dor C, the low mass companion to AB Dor A. By effectively eliminating all contamination from AB Dor A, the extracted spectrum retains both continuum and spectral features. The achieved 1σ contrast is 9 mag at $0''.2$, 11 mag at $0''.5$, in 20 mins exposure time, at an effective spectral bandwidth of 5.5 nm, proving that the method is applicable even in low Strehl regimes.

The spectral deconvolution method clearly demonstrates the efficacy of image slicer based IFUs in achieving very high contrast imaging spectroscopy at small angular separations, validating their use as high contrast spectrographs/imagers for extreme adaptive optics systems.

Key words: instrumentation:spectrographs (integral field) – instrumentation: adaptive optics – techniques:high contrast – image slicers – extrasolar planets – stars:individual (AB Doradus C)

1 INTRODUCTION

Direct imaging and spectroscopy of extra-solar planets is a research area that has attracted significant attention in recent years. Several specialised instruments are now being designed and built to achieve this goal within the next few years (e.g. VLT Planet Finder (SPHERE) – Beuzit et al. (2006), Gemini GPI – Soummer et al. (2006), Keck XAOPI – Macintosh et al. (2004)). The major difficulty in detecting exo-planets is the extreme contrast between the star (typically a main-sequence M–G dwarf) and the planet (typically less than $1''$ away). Even in the most favourable conditions, theoretical computations (e.g. Burrows et al. 2004)

have shown that the brightness ratio between the parent star and the exo-planet is expected to be at least 15 magnitudes at $1''$. Such contrasts are significantly beyond normal imaging techniques even with the best adaptive optics systems available today. If we are to attain this ambitious goal, novel ways to maximise the achieved contrast must be devised.

Even in high-Strehl AO systems, long exposures do not provide a smooth halo around the central star, as one would expect from a time average of the speckles caused by atmospheric turbulence. In fact, due to the presence of super-speckles, imaging contrasts are much worse than the theoretical *photon noise* limit (Racine et al. 1999). Super-speckles (also called quasi-static speckles Marois et al. (2006)) are long lived speckles caused by imperfections in the light path, and have coherence times ranging from tens of seconds to several minutes. Any changes in the light path, for example

^{*} Based on observations collected at the European Southern Observatory, Chile, under ESO programme 276.C-5013.

due to instrument flexure or changing telescope position, cause the super-speckles to vary, making it impossible to remove them with static calibrations obtained at a different time (e.g. PSF star observations will show a completely different super-speckle pattern).

The contrast limitations posed by super-speckles can only be overcome through *simultaneous* observations. Several techniques have been proposed to achieve this (e.g. Guyon 2004; Marois et al. 2004, 2006; Ren & Wang 2006) including the “spectral difference imager” (SDI) technique developed by one of the authors (Lenzen et al. 2004) and others (Marois et al. 2005). The technique utilises the fact that the planetary spectrum has sharp, deep absorption features (e.g. CH₄ in the H band) to dramatically improve the contrast with respect to scattered starlight, which has a smooth spectrum. By taking simultaneous images in and out of the methane absorption band, and scaling and subtracting the two images, one effectively removes the starlight, while leaving the planetary light intact. The subtraction removes residual starlight, whether in the form of rapidly time-varying speckles, slowly varying super-speckles, or any other form of scattered light within the telescope & instrument. In fact, the SDI technique uses an ingenious double-difference, so as to further reduce any residuals arising from systematic errors due to differing optical paths. Biller et al. (2006) have demonstrated the success of SDI in finding cool companions with the NACO instrument on the ESO-VLT.

SDI is however limited in application as it relies on an intrinsic feature of the companion spectrum; the CH₄ absorption feature only found in objects with $T_{\text{eff}} < 1200$ K. In addition, there is a need for follow-up spectroscopy of the candidate object detected – both to confirm its nature (often via common proper motion with the parent), and to characterise it in detail. In this paper, we describe an extension of the Sparks & Ford (2002) *spectral deconvolution* (SD) technique to achieve high-contrast imaging (and spectroscopy) with an integral field spectrograph (IFS). This technique does not rely on any feature of the target object’s spectrum and is therefore applicable to any high contrast imaging application. In addition, the use of an IFS provides a complete dataset in one go, and with maximum signal-to-noise (no slit losses). Furthermore, complete 2D spatial information allows the continuum to be correctly measured, in contrast to extremely narrow slits needed for A.O. assisted spectroscopy. No a-priori information about the spatial location of the companion is needed either, an inherent advantage of using an IFS.

The next two sections describe the Sparks & Ford (2002) method, as well as proposed extensions, including using this technique at small inner working radii (within the bifurcation radius, see section 2.2), and in section 3 we provide a demonstration of the achievable performance in this regime, *even without a coronagraph*. Section 3.4 presents the results and section 4 elaborates on the future prospects and the discovery potential for high contrast imaging spectroscopy with image slicer based integral field spectrographs, utilising this technique.

2 CONCEPT

Several authors (e.g. Sparks & Ford 2002; Fusco et al. 2005; Berton et al. 2006) have suggested that the wealth of spectral information available in an IFS data cube can be utilised to remove scattered starlight and identify the presence of a close-in companion, and extract its spectrum with enhanced signal-to-noise (SNR), thus maximising contrast. Our scheme is an extension of the spectral deconvolution technique proposed by Sparks & Ford (2002), adapted to ground based observing with both extreme adaptive optics and general purpose adaptive optics systems, and further optimised to maximise SNR. Application of the concept to ground based IFS fed by general purpose A.O. systems is very challenging, as the Strehl ratio is typically only ~ 0.5 , and varies strongly with wavelength.

The central tenet of the SD technique is that the position of almost all features arising from the parent star (Airy pattern, speckles, etc.) scale smoothly and slowly with wavelength (e.g. the first Airy null is always $1.22 \lambda/D$ from the star), whereas a physical object’s location is independent of wavelength. Thus, stepping through the wavelength axis of an IFS data cube at a fixed spatial location (e.g. the location of a companion), one would see a modulation arising from maxima and minima of the Airy pattern passing through the companion’s location (see figure 24 in Sparks & Ford 2002). These modulations would drown out any expected signal from the companion. If however, we use the wavelength dependence to advantage, we can effectively subtract all wavelength dependent artifacts in the stellar point spread function (PSF), thus unmasking the presence of real physical objects.

The technique is best illustrated via the removal of the Airy pattern from the IFS data cube, although it applies equally well to any *achromatic* aberration in the wavefront. Each wavelength slice of the IFS data cube is scaled radially, so as to exactly compensate the wavelength dependence of the Airy pattern. Nulls and maxima in the Airy pattern, which used to be located at different radial distances in the different wavelength slices now line up perfectly at all wavelengths in the scaled data cube (e.g. figure 27 in Sparks & Ford 2002). The companion’s light now traces a diagonal line through the data cube.

Sparks & Ford (2002) fit a low order polynomial to every spatial pixel (spaxel¹) of the data cube, while rejecting outliers. The result is a very high SNR estimate of the Airy pattern (and all wavelength dependent speckles) at each wavelength of the data cube. The faint companion represents a high frequency modulation and is thus excluded from the low order polynomial fit (as it represents a tilted line through the scaled data cube, it is present in any given spaxel over only a small range of wavelengths). The light from the parent star is then subtracted from each scaled slice of the data cube, and the result scaled back to the original grid, to form the result cube.

The actual implementation of the concept for ground based A.O. assisted integral field spectroscopic data (without a coronagraph) has to account for low Strehl that varies

¹ The term spaxel describes all pixels spanning the entire wavelength range of an IFS data cube that correspond to a single spatial pixel

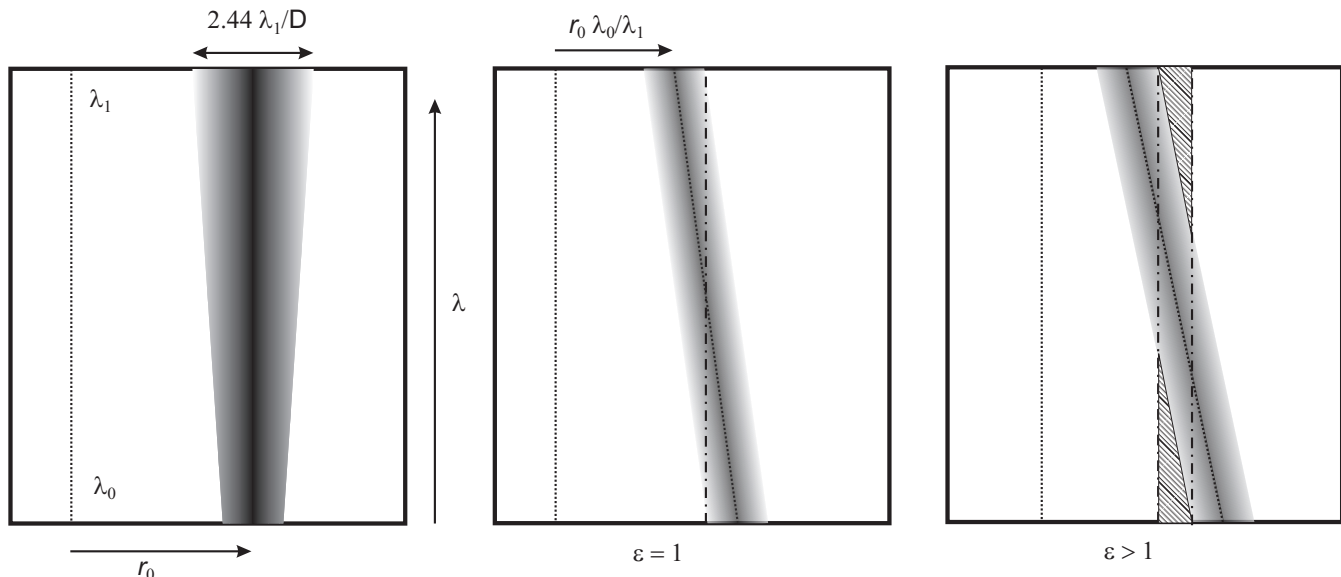


Figure 1. The left hand panel is a schematic of a slice through the IFS data cube, in the $x - \lambda$ plane, with the x axis along the line joining the centre of the star with the centre of the faint companion. The dotted line represents the peak of the stellar light profile (as a function of λ). The size of the companion, quantified as $2.44\lambda_1/D$, increases with wavelength. The middle panel shows the data cube scaled inversely with wavelength, centred on the star. The faint companion's separation is such that $\epsilon = 1$. The collapsed cube will be contaminated by companion light at all r values. The right hand panel illustrates the situation for $\epsilon > 1$, where the hatched areas represent parts of the data cube not contaminated by light from the companion. It is thus possible to create a collapsed image free from companion light.

substantially with wavelength. Furthermore, we have extended the original concept in two ways: (a) to extract spectra from objects that lie close to the parent star and (b) optimise the signal to noise ratio of the extracted spectra. We elaborate on these extensions in the following sub-sections.

2.1 Application to faint companions at small separations

The SD technique utilises the wavelength dependence of PSF features to obtain a high signal-to-noise estimate of the parent star PSF, while rejecting the light from the faint companion. We first derive the limiting distance for which the technique is applicable in its original proposed form, and then explain how we deal with close-in companions.

2.2 Bifurcation point for characterisation analysis

Consider a companion object located at radial distance r (expressed in angular units) from the primary object, imaged with a telescope of diameter D . The distance to the first null of the Airy pattern is given by the usual formulation

$$\Theta_0 = 1.22 \frac{\lambda_0}{D} \quad (1)$$

where λ_0 is the shortest wavelength in the IFS data cube. Defining the object extent as equal to $2\Theta_0$, and the wavelength range of the IFS as extending from λ_0 (shortest) to λ_1 (longest), we obtain an expression for the movement of the companion's centre in the scaled data cube as

$$\Delta r = r - r \frac{\lambda_0}{\lambda_1} = r \frac{\Delta\lambda}{\lambda_1} \quad (2)$$

Noting that the extent of the object stays constant in the scaled data cube, we can then express the bifurcation point as

$$\Delta r = r \frac{\Delta\lambda}{\lambda_1} = 2\epsilon \times 1.22 \frac{\lambda_0}{D} \quad (3)$$

where ϵ is a factor slightly greater than one. The parameter ϵ is explained in figure 1.

For $\epsilon \equiv 1$, the scaled data cube is entirely contaminated by light from the companion, but only just so. For $\epsilon > 1$, a *clean* collapsed image devoid of flux from the companion object can be made by collapsing a small fraction of wavelength channels at either end of the data cube. This is only necessary in the near vicinity of the faint companion, as shown by the hatched areas in the right hand panel of figure 1.

The amount by which ϵ must exceed unity depends on the SNR of the observation, as sufficient number of wavelength channels must be used to form the high SNR PSF estimate. Table 1 lists values of the bifurcation point for typical near-infrared band passes for an 8 meter telescope, for a couple of typical values of ϵ . It is obvious from the table that extended wavelength coverage by the IFS is crucial for removing the flux from a close-in companion in the scaled data cube.

2.3 Extension to close-in faint companions

We have extended the SD technique to close-in faint companions by using an iterative technique to remove the faint companion's light from the PSF estimate made using the scaled data cube. Residual light from the faint companion in the estimated PSF will reduce the flux level of the compan-

Table 1. Bifurcation point in the data reduction as a function of bandpass of observations and factor ϵ . r is the value of the bifurcation radius in milli-arcseconds.

Band	λ_1 μm	λ_2 μm	ϵ	r mas
H	1.45	1.8	1.1	516
K	1.95	2.45	1.1	661
H+K	1.45	2.45	1.1	246
H	1.45	1.8	1.2	563
K	1.95	2.45	1.2	721
H+K	1.45	2.45	1.2	268

ion in the final result cube. Furthermore, due to the wavelength scaling process, any residual light will affect spectral channels differently, resulting in an error in the continuum slope of the derived faint companion spectrum. Section 3 shows that both the total flux and the continuum slope were correctly measured for the observations reported here, thus proving the efficacy of the proposed extension to the SD technique.

The following assumes that the position of the close-in faint companion is already known (section 3.4 mentions how this might be derived from the IFS data cube itself). The companion is also assumed to be an unresolved point source, with a full width at half maximum (FWHM) roughly equal to the diffraction limited FWHM for the telescope aperture in question.

Knowing both the position and the size of the source, we fit for the companion amplitude and background level in individual spectral channels of the observed data, prior to scaling. Subtracting an ideal Airy pattern centred on the primary improves the robustness of the fit, as does averaging ~ 10 spectral channels. Scatter in the fit parameters is further reduced by describing each fit parameter with a low order polynomial as a function of wavelength. The goal is to remove most of the flux from the faint companion, the quality of the fit need not be very good. The SD technique is then applied to the data cube from which the faint companion light has been removed, to first order.

The result data cube will contain residual companion flux due to inaccuracies in the fit. However, as most of the PSF features will have been eliminated by the spectral deconvolution process, we can use the result data cube as a starting point for a second iteration, fitting the faint companion more accurately than in the initial step. After subtracting the improved estimate of the faint companion light from the observed data cube, we apply the SD method again (second iteration) to obtain an improved result cube. Further iterations are carried out until convergence is achieved, and the extracted spectrum of the faint companion does not change. Fit parameters such as companion position and width, fixed at first, can be free parameters in subsequent iterations to improve the quality of the fit. We applied this iterative technique to the data presented in the next section, and found that only two iterations were required to achieve convergence.

The key to successfully applying the iterative procedure is to produce a reasonable, if noisy, estimate of the faint companion flux in the first iteration. This can be achieved

by subtracting an ideal Airy pattern centred on the primary, or by subtracting data taken with the same instrument, but with a different rotator angle. In either case, the purpose is to estimate and remove the azimuthally symmetric component of the PSF, so as to enhance the contrast at the location of the faint companion. This can also be achieved by fitting a radial profile to the primary’s light distribution, and subtracting it from the observed data cube. The radial profile can also be used to model the flux distribution from the faint companion, resulting in a better subtraction of the companion flux in the data processing.

For faint companions located further than the bifurcation point, applying the iterative procedure outlined above can still improve the SNR of the final extracted spectra, as it reduces the contamination from the faint companion light in the PSF estimate.

2.4 Optimising the SNR of the extracted spectra

Observations carried out with a general purpose A.O. system suffer from the added complication of moderate Strehl that varies substantially with wavelength. Consequently, the FWHM of the PSF does not scale with λ as expected for a purely diffraction limited system. Instead, with Strehl increasing with wavelength, the PSF is too broad at the shortest wavelengths, and too narrow at the longest wavelengths, a feature which persists in the scaled data cube. This results in a radial distance and wavelength dependent flux residual after applying the SD technique. Consequently, the continuum of the faint companion is incorrectly determined. To rectify these errors caused by the varying Strehl, we fit and subtract a radial profile for the primary light from each spectral channel of the data cube prior to applying the SD technique. The data presented in section 3 have been so treated.

A further improvement in SNR of the extracted spectrum is obtained by scaling the PSF estimate cube back to the original observed pixel scale and subtracting it from the observed data cube, rather than scaling the observed data cube and performing the subtraction of the scaled cubes. Although the scaling is a linear operation, an interpolation is performed to place all scaled channels on a common grid, and this results in noise enhancement. As the observed data have much lower SNR (per spectral channel) than the PSF estimate formed by the SD technique, the noise enhancement is avoided almost completely by scaling and de-scaling the high SNR PSF estimate rather than the lower SNR observed data cube.

3 DEMONSTRATION

We obtained observations of the local young K-dwarf AB Doradus, which is known to have a M-dwarf companion (AB Dor C) with $\Delta K=5$ magnitudes only $0'.2$ away (Close et al. 2005). AB Dor A has a K-band magnitude of 4.6, making it an ideal AO guide star. Details of the AB Dor C observations and data analysis are presented here as proof-of-concept of the proposed extensions to the SD technique, as described in previous sections. It is also the first time the SD method has been applied to a ground based A.O. assisted IFS data set, with moderate Strehl and no coronagraph present. As

Table 2. List of observations. All observations were made with the H+K grating. The 250 mas observations will not be discussed in this paper.

Target	Spaxel Size (mas)	DIT (s)	NDIT	Total exposure (s)
AB Dor ^a	25	5.0	16	1280
AB Dor ^b	25	5.0	16	1280
AB Dor ^c	250	0.83	4	6.64
Teide 1 ^d	250	300	1	600

^a-16.5deg PA

^b+16.5deg PA

^cThese data were taken to bootstrap the spectral PSF from 250 mas pixel scale to the 25 mas pixel scale, if required

^dFull designation is Cl* Melotte 22 Teide 1, template of M8 spectral type

such, it also serves as an experimental verification of the SD method and its applicability to ground based data sets. We also present a high SNR H & K band spectrum of AB Dor C extracted using this technique. Further detailed analyses of the results of these observations are published in the companion paper by Close et al. (2007) (Paper II).

3.1 Observations

Data were obtained on the nights of 24th and 25th January 2006 with the SINFONI instrument (Thatte et al. 1998; Eisenhauer et al. 2003; Bonnet et al. 2004) at the Cassegrain focus of the ESO VLT-UT4 (Yepun). Table 2 lists the observations, all with the H+K grating. DIT is the time per exposure, NDIT such exposures are averaged together by the readout hardware, and the result is written to disk. The total exposure time is made up of many such averaged frames. In addition to the AB Dor system, observations were made of a star in the Pleiades cluster to serve as an M8 template of young age, and of several telluric standards, at both 25 and 250 mas plate scales.

AB Dor A was used as the guide star for the SINFONI adaptive optics module (Bonnet et al. 2004). The mean Strehl ratio delivered was 0.37 on the 25th, and 0.35 on the 26th, as reported by the SINFONI A.O. system itself. SINFONI was used in the 25 mas scale to ensure adequate sampling of the PSF. To enable removal of bad pixels, and to sample SINFONI’s rectangular spaxels, a dither pattern with offsets of exactly ± 0.5 spaxels was used. The H+K grating was used to maximise the wavelength coverage, resulting in a spectral resolving power of ~ 1500 , and instantaneous wavelength coverage of $1.4\mu\text{m} - 2.45\mu\text{m}$. No blank sky observations were taken for AB Dor at the 25 mas pixel scale, as it was clear that the data would be dominated by photon/speckle noise from AB Dor A. The J band was used for acquisition to avoid saturation of the detector array. Seeing during the observations (as reported by the Atmospheric Site Monitor) varied between $0''.58$ and $0''.74$, with a mean of $0''.64$ on the 25th, and between $0''.61$ and $0''.86$ with a mean value of $0''.69$ on the 26th.

3.2 Data reduction

Basic data reduction followed the standard SINFONI data reduction procedure, outlined in Schreiber et al. (2004) & Abuter et al. (2006), with extensions to deal with the 2K camera upgrade of February 2005 (Eisenhauer et al. 2002). The jitter pattern was corrected by combining data cubes, one for each on-source exposure recorded, creating a single mosaicked cube with a total observing time of 20 minutes for the data of the 25th, and a second one (with different rotator angle) for the 26th. Accurate centroiding of AB Dor A in the resulting data cube showed a residual variation with wavelength, implying that the standard differential atmospheric refraction correction employed by the pipeline reduction was not accurate enough. Consequently, we disabled the differential atmospheric refraction correction in the standard reduction, and did a post-correction of the AB Dor A centroid movement along the wavelength axis of the data cube, using a cubic polynomial function. The resulting improved model for differential atmospheric refraction will be presented elsewhere.

It should be noted that even after disabling the differential atmospheric refraction correction, there are still three interpolations inherent in the production of a SINFONI data cube, two of which use a nearest neighbour interpolation algorithm with a tanh kernel, and one uses a polynomial interpolation algorithm. One interpolation is required to “straighten” the spectra, a second does re-gridding onto an uniform grid in wavelength, and a third corrects for sub-pixel shifts between slices. We have not evaluated the impact of these interpolations in a quantitative manner, but it is likely that they do impact the maximum contrast achieved by these observations.

Implementation of the SD technique (and its extensions) used both IDL and GIPSY data analysis packages, in addition to the routines from the SINFONI pipeline. GIPSY (Vogelaar & Terlouw 2001) was used primarily for visualisation of the data cubes with `sliceview`, while most computationally intensive tasks were performed in IDL.

3.3 The SD technique and extensions

AB Dor C is located $0''.2$ from AB Dor A, at P.A. 181° at the epoch of these observations, based on orbit parameters determined by Nielsen et al. (2005). Using equation 3, we note that AB Dor C is closer than the bifurcation radius, thus requiring an iterative procedure to identify the companion and extract its spectrum.

The technique described in previous sections was applied to the AB Dor data cubes to extract a spectrum of the companion AB Dor C. As AB Dor C is clearly visible in the raw data cube (see figure 2), there was no problem in determining the companion location. However, AB Dor C did overlap with a bright spot in the diffraction pattern in the data taken on the 25th. The pattern of four bright spots is caused by the telescope secondary mount diffraction pattern superposed on the Airy pattern. Consequently, accurate determination of the companion location did require a second iteration of the SD technique, as explained in section 2.3 above. Due to the strong dip in atmospheric transmission at the edges of both H and K bands, the processing was confined to wavelength ranges 1.457 to $1.80\mu\text{m}$ and 1.95 to

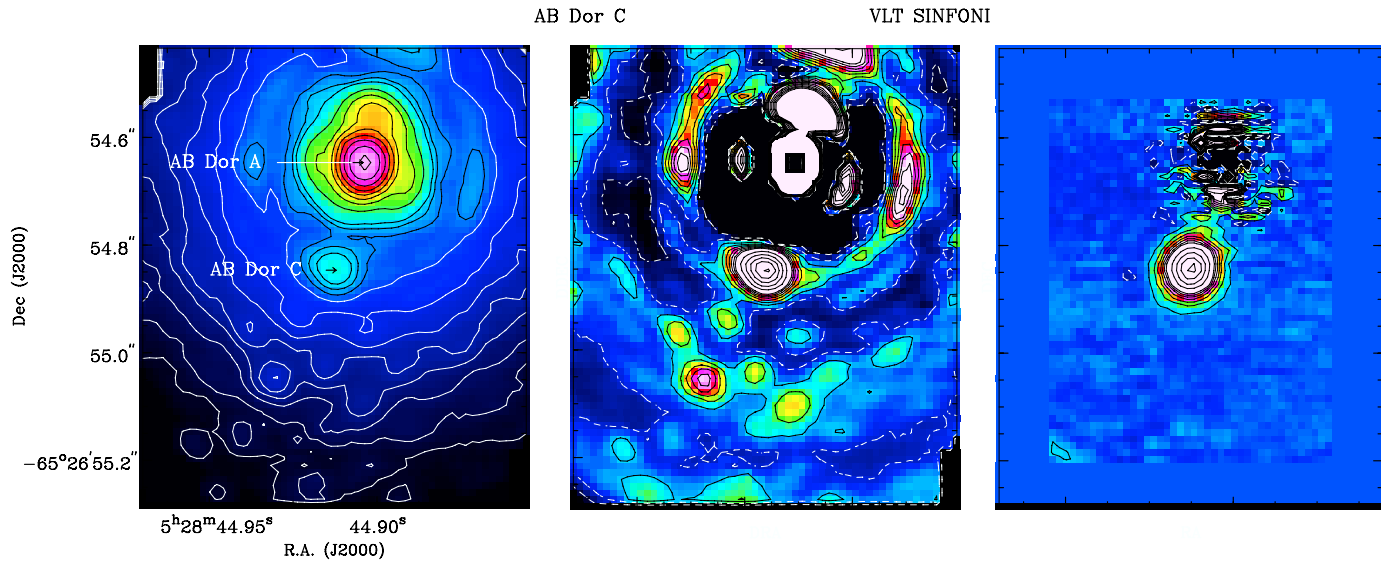


Figure 2. Illustration showing the efficacy of the SD technique at removing both PSF artifacts and super-speckles from the SINFONI IFS data cube for the AB Dor system. The left frame shows one wavelength slice of the observed data cube at $2.2 \mu\text{m}$. Note that the entire vertical extent of the image is only $0''.9$. The colour table is logarithmic (min 10^1 , max 10^4). The contours are logarithmic, from 0.9 to 2.3 in steps of 0.1, and from 2.3 to 4.0 in steps of 0.2. The middle frame shows the same data, but with a radial profile fitted and subtracted, so as to highlight the PSF imperfections. The super-speckles are easily confused with real sources in this narrow-band image. The colour table is now linear (min -10, max 25), with contours from -12.5 to 32.5 in steps of 5, and from 32.5 to 150 in steps of 20. The four-fold symmetry of the Airy pattern arises from the superposition of the diffraction spikes from the secondary support structure on the Airy rings. The right hand frame shows the same wavelength slice of the data cube, after applying the SD technique iteratively. Colour table and contours are the same as for the middle frame. Super-speckles are completely absent at the lowest contour level of ± 2.5 , corresponding to a 1σ error of ≤ 1 unit.

$2.45 \mu\text{m}$ respectively for the H and K bands. A total of two iterations were needed for the SD technique to yield a high SNR PSF estimate free from companion flux.

3.4 Results

Figure 2 shows one wavelength slice of the SINFONI IFS data cube for the AB Dor system before and after the application of the SD technique (and its extensions) described above. The separation of AB Dor C from the parent was only $0''.2$ at this epoch, while the flux contrast was $\Delta m = 4.90$. The left hand frame shows the raw data, while the central frame has a smooth radial profile fitted and subtracted from the raw data to highlight the PSF artifacts, and in particular, the super-speckles. The right hand frame shows the result of applying the technique described in section 2. We can successfully remove both Airy pattern residuals, as well as super-speckles. Note the four-fold symmetry of the Airy pattern, a result of the superposition of the Airy ring with the diffraction from the spider arms of the secondary. Unfortunately, AB Dor C is located at the same orientation as one of the Airy peaks. We prefer to use this data set as it has significantly better Strehl, although the other data set (rotated by 33°) places AB Dor C at a more favourable location relative to the Airy peaks. Stepping through the data cube along the wavelength axis, all PSF imperfections scale linearly with wavelength,² while the real object stays

at a fixed location. The data do demonstrate that the SD technique can effectively separate companion and PSF contributions, even if they are spatially coincident in a single wavelength channel. The removal of the super-speckles is of particular value, as their shape mimics point sources in the field in any narrowband image.

3.4.1 Extracted spectra of AB Dor C

Figures 3 and 4 shows the normalised, extracted spectra of AB Dor C, using the SD technique. The data have been smoothed with a boxcar of width 3 pixels, corresponding to 1.5 nm. The SNR of the K band spectrum exceeds 40, as derived from the contrast values discussed in 3.4.2. The quality of the spectrum is limited by systematic errors in the division of telluric features, as no sky observations were performed. The NACO spectrum previously obtained by Close et al. (2005) at a tighter $0''.15$ separation is also shown for comparison. Note that the SD technique is able to reproduce not only the spectral features but the continuum slope as well, in contrast to A.O. long-slit measurements with varying slit filling factors. The output data cube, after applying the SD technique, is used to measure the position, flux, and spectral type of AB Dor C. At the epoch of these observations, AB Dor C was located 201.7 ± 10 milli-arcseconds from AB Dor A, at P.A. 180.78° . The K magnitude was 4.90 mag fainter than AB Dor A, which, combined with the 2MASS measurement for AB Dor A yields $K=9.59$ for AB Dor C. A spectral type of $M5.5 \pm 0.5$ can be derived by comparing the observed spectrum with young and old templates. A detailed analysis of the properties of AB Dor C (including its spec-

² mpeg movies of the raw, radial profile subtracted and SD result data cubes can be viewed at <http://www-astro.physics.ox.ac.uk/~thatte/abdorc>

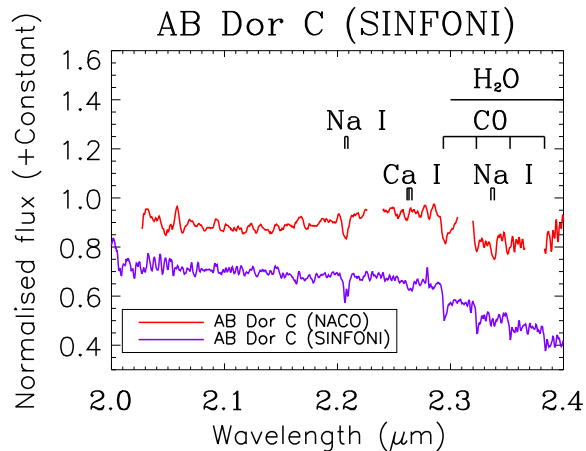


Figure 3. The K band extracted spectrum of AB Dor C, with some of the prominent stellar features marked. The K band spectrum obtained by NACO A.O. long slit spectroscopy, at $0''.150$ separation (Nielsen et al. 2005) is also shown for comparison. Note that our spectrum also correctly recovers the continuum slope, vital for deriving the spectral type of this young object (see Paper II for details of the spectral classification). The “emission” feature just shortward of the first CO bandhead is a residual telluric feature that was not correctly subtracted out.

tral type determination) is presented in Paper II. Note that both the companion flux and its spectral continuum slope are correctly derived using the iterative method described in section 2.3 above.

3.4.2 Achieved Contrast

The remarkable success of the SD technique at removing light contamination resulting from PSF imperfections is illustrated in figure 5. The plot shows the resulting radial profile for a 20 min exposure of the AB Dor system observed with SINFONI, with a spectral width of 5.5 nm, using the SD technique. AB Dor C is clearly visible as a bump in the radial profile at $0''.2$. The curve shows the contrast achieved (1σ) is ~ 9 mag at $0''.2$, and 11 mag at $0''.5$, without using a coronagraph. Note that the effective spectral resolution ($R=400$) is higher than that achieved by SDI ($R=50$) (Lenzen et al. 2004; Biller et al. 2006). The achieved contrast is still ~ 1 mag from the photon noise limit, although we suspect that some residual noise is attributable to non-optimal interpolations in the data reduction procedure, and can be improved upon. The ultimate limitations of the technique will be addressed in a separate paper.

3.5 Faint object detection

AB Dor C is only 5 mag fainter than AB Dor A, and could thus be easily detected in the raw data cube. However, we note that the SD technique can also be used for detection of faint companions. Any feature whose radial distance from the primary does not scale with wavelength generates a radial streak in a collapsed image created by averaging the scaled data cube along the spectral dimension. Subtracting the collapsed image (scaled back appropriately for each

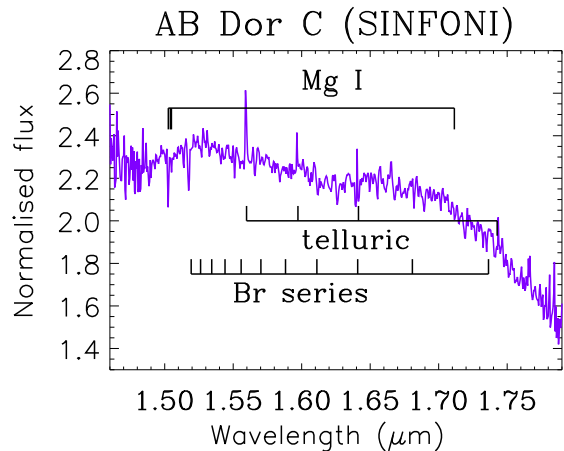


Figure 4. The H band extracted spectrum of AB Dor C, with some of the stellar features marked. Also marked are the location of the Brackett series hydrogen recombination lines, as these were present in absorption in the late B telluric standard. Although every effort was taken to accurately fit these lines, some residuals remain. As no sky observations were made, some of the brightest night sky OH emission lines are also present in the derived spectrum. The H and K spectra were obtained simultaneously, by applying the SD technique (and its extensions) to the data cube covering both H & K bands. They are shown separately for clarity.

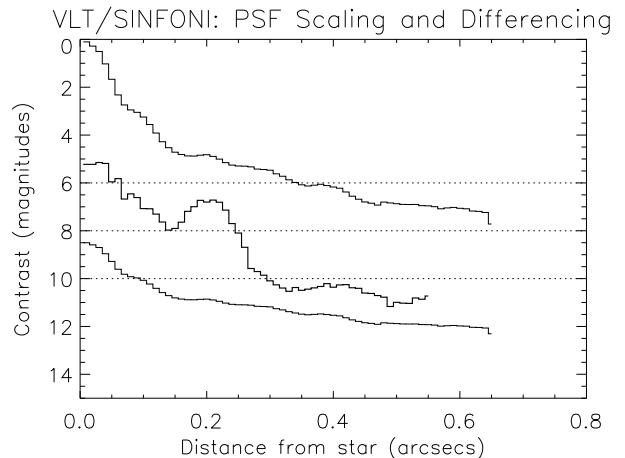


Figure 5. The plot shows three curves - the top curve is the radial profile of AB Dor A. The bottom curve is the square root of the top curve, so it represents the photon noise limit. The middle curve is the standard deviation in the SD result frame, so it is a measure of the residual noise. The horizontal lines at 6, 8 and 10 magnitudes are for reference. The large bump at $0''.2$ in the SD result frame is due to AB Dor C. The achieved contrast is 9 mag at $0''.2$, and 11 mag at $0''.5$, in 20 mins exp. time at $R_{\text{eff}}=400$. As no coronagraph is used, very high contrasts can be obtained at small inner working radii.

wavelength) from the original data cube results in a diminished companion flux plus an inward negative streak at the shortest wavelengths, a diminished flux companion plus a symmetric negative radial streak at central wavelengths, and a weaker companion plus an outward negative streak at the longest wavelengths. The final collapsed image shows the characteristic pattern of a positive object sitting atop a long negative radial streak centred on the object ((see both “planets” in fig. 26 of Sparks & Ford 2002)). This characteristic pattern can be used to detect faint companions. Furthermore, if the primary’s radial light profile is fitted and subtracted from each wavelength slice of the data cube prior to applying the SD technique, the contrast of the faint companion can be further enhanced.

If the technique is applied to data cubes taken at two different rotator angles and subtracted from each other prior to step 1, only features that are stationary on the sky will remain. In addition to showing the characteristic pattern described above, they will also show a positive and negative image of true celestial objects, separated by the difference in rotator angles. The resulting pattern can be easily used to identify potential faint companions.

4 CONCLUSIONS

In this paper we have introduced extensions to the SD technique proposed by Sparks & Ford (2002) for achieving high contrast imaging spectroscopy with an AO-fed integral field spectrograph at small inner working radii. Applying this technique to real data, we have shown it to provide very high contrast spectra of faint companions very close to bright stars. The achieved contrast is substantially better than previously achieved by other techniques, especially as no coronagraph was used. The absence of a coronagraph removes limits on the smallest inner working radius, especially valuable as most exo-planet candidates are expected to lie at very small separations from the parent star. The SD technique holds great promise for direct imaging of exo-planets, as it simultaneously detects and spectrally characterises any faint companion, thus removing the need for expensive and time-consuming follow-up observations, either to detect common proper motion or to obtain a spectrum of the faint companion. In addition, the technique does not require any assumptions about the companion’s spectral characteristics (e.g. presence of a CH₄ feature), and can therefore be applied to any high contrast application.

Our demonstration of the efficacy of the SD technique to obtain spectra of the close-in faint companion AB Dor C shows that image slicer based integral field spectrographs are capable of achieving very high contrasts, contrary to the expectations of several groups (Claudi et al. 2004; Verinaud et al. 2006; Berton et al. 2006) who were concerned that large non-common-path errors would limit the contrast achievable with these systems. The SINFONI IFS design (Tecza et al. 2000, 2003) exclusively uses classically polished flat glass mirrors in its image slicer, thus achieving very small non common path errors, as demonstrated here. Indeed, we have shown that an integral field spectrograph alone can provide a large fraction of the total contrast requirement of an exo-planet direct detection instrument.

Successful application of the SD technique requires large instantaneous wavelength coverage, strongly favouring image slicer based IFS designs. These naturally provide large simultaneous wavelength coverage, while it is rather difficult to achieve a large bandwidth in lenslet array based designs. The requirement to keep non common path errors to an absolute minimum strongly favours image slicer designs with classically polished glass slicing optics (not just slicing mirrors, but the entire slicer optics), as implemented in the SINFONI spectrograph (Tecza et al. 2000, 2003).

5 ACKNOWLEDGEMENTS

We thank the ESO Director-General for allocating Director’s discretionary time to carry out these observations. We thank MPE for use of the *spread* SINFONI data reduction software. This paper is based on observations collected at the European Southern Observatory, Chile under ESO programme ID 276.C-5013. NT, FJC & MT are funded through Marie-Curie Excellence Grant MEXT-CT-2003-002792. EN is supported by a Michelson Fellowship. LMC is supported by an NSF CAREER award and the NASA Origins of Solar Systems program. We thank the referee, W.B.Sparks for extensive comments that greatly improved the paper.

REFERENCES

- Abuter R., Eisenhauer F., Schreiber J., Horrobin M., Genzel R., Davies R., Lehnert M., Tecza M., 2006, *New Astronomy Review*
- Berton A., Feldt M., Gratton R., Hippler S., Henning T., 2006, *New Astronomy Review*, 49, 661
- Berton A., Gratton R. G., Feldt M., Henning T., Desidera S., Turatto M., Schmid H. M., Waters R., 2006, *ArXiv Astrophysics e-prints, astro-ph/0605207*
- Beuzit J. L., Mouillet D., Moutou C., Dohlen K., Fusco T., Puget P., Udry S., Gratton R., Schmid H. M., Feldt M., Kasper M., The Vlt-Pf Consortium 2006, in Arnold L., Bouchy F., Moutou C., eds, *Tenth Anniversary of 51 Peg-b: Status of and prospects for hot Jupiter studies A “Planet Finder” instrument for the VLT.* pp 353–355
- Billier B. A., Close L. M., Lenzen R., Brandner W., McCarthy D., Nielsen E., Kellner S., Hartung M., 2006, in Aime C., Vakili F., eds, *Direct Imaging of Exoplanets: Science & Techniques. Proceedings of the IAU Colloquium #200*, Edited by C. Aime and F. Vakili. Cambridge, UK: Cambridge University Press, 2006., pp.571-576 Suppressing Speckle Noise for Simultaneous Differential Extrasolar Planet Imaging (SDI) at the VLT and MMT. pp 571–576
- Bonnet H., Abuter R., Baker A., Bornemann W., Brown A., Castillo R., Conzelmann R., Damster R., 2004, *The Messenger*, 117, 17
- Bonnet H., Conzelmann R., Delabre B., Donaldson R., Fedrigo E., Hubin N. N., Kissler-Patig M., Lizon J.-L., Pauflique J., Rossi S., Stroebele S., Tordo S., 2004, in Bonaccini Calia D., Ellerbroek B. L., Ragazzoni R., eds, *Advancements in Adaptive Optics.* Edited by Domenico B. Calia, Brent L. Ellerbroek, and Roberto Ragazzoni. Proceedings of the SPIE, Volume 5490, pp. 130-138

- (2004). First light of SINFONI AO-module at VLT. pp 130–138
- Burrows A., Sudarsky D., Hubeny I., 2004, *ApJ*, 609, 407
- Claudi R. U., Turatto M., Gratton R., Antichi J., Buson S., Pernechele C., Desidera S., Baruffolo A., 2004, in Moorwood A. F. M., Iye M., eds, *Ground-based Instrumentation for Astronomy*. Edited by Alan F. M. Moorwood and Iye Masanori. *Proceedings of the SPIE*, Volume 5492, pp. 1351-1361 (2004). CHEOPS NIR IFS: exploring stars neighborhood spectroscopically. pp 1351–1361
- Close L. M., Lenzen R., Guirado J. C., Nielsen E. L., Marmajek E. E., Brandner W., Hartung M., Lidman C., Biller B., 2005, *Nature*, 433, 286
- Close L. M., Thatte N., Nielsen E. L., Abuter R., Clarke F. J., Tecza T., 2007, *ArXiv Astrophysics e-prints*, astro-ph/0703564
- Eisenhauer F., Abuter R., Bickert K., Bonnet H., Brynnel J., Conzelmann R., Delabre B., Donaldson R., Farinato J., Fedrigo E., Genzel R., Iserlohe C., Kasper M., Roehrl C., Schreiber J., Tecza M., Thatte N., 2003, in *Instrument Design and Performance for Optical/Infrared Ground-based Telescopes*. Edited by Iye, Masanori; Moorwood, Alan F. M. *Proceedings of the SPIE*, Volume 4841, pp. 1548-1561 (2003). SINFONI - Integral field spectroscopy at 50 milli-arcsecond resolution with the ESO VLT. pp 1548–1561
- Eisenhauer F., van der Werf P., Thatte N., de Zeeuw T., Tecza M., Franx M., Iserlohe C., 2002, in *Bergeron J., Monnet G., eds, Scientific Drivers for ESO Future VLT/VLTI Instrumentation: Proceedings of the ESO Workshop Held in Garching, Germany, 11-15 Juni 2001, ESO ASTROPHYSICS SYMPOSIA*. ISBN 3-540-43755-X. Edited by J. Bergeron and G. Monnet. Springer-Verlag, 2002, p. 149 *Scientific Potential of Enhancing the Integral-Field Spectrometer SPIFFI with a Large Detector and High Spectral Resolution*. pp 149–+
- Fusco T., Rousset G., Beuzit J.-L., Mouillet D., Dohlen K., Conan R., Petit C., Montagnier G., 2005, in *Focal Plane Arrays for Space Telescopes II*. Edited by Grycewicz, Thomas J.; Marshall, Cheryl J. *Proceedings of the SPIE*, Volume 5903, pp. 148-159 (2005). Conceptual design of an extreme AO dedicated to extra-solar planet detection by the VLT-Planet Finder instrument. pp 148–159
- Guyon O., 2004, in *Advancements in Adaptive Optics*. Edited by Domenico B. Calia, Brent L. Ellerbroek, and Roberto Ragazzoni. *Proceedings of the SPIE*, Volume 5490, pp. 593-601 (2004). Synchronous interferometric speckle subtraction (SISS): a concept to remove speckle noise in adaptive optics imaging and interferometry. pp 593–601
- Lenzen R., Close L., Brandner W., Biller B., Hartung M., 2004, in *Ground-based Instrumentation for Astronomy*. Edited by Alan F. M. Moorwood and Iye Masanori. *Proceedings of the SPIE*, Volume 5492, pp. 970-977 (2004). A novel simultaneous differential imager for the direct imaging of giant planets. pp 970–977
- Macintosh B. A., Bauman B., Wilhelmsen Evans J., Graham J. R., Lockwood C., Poyneer L., Dillon D., 2004, in *Bonaccini Calia D., Ellerbroek B. L., Ragazzoni R., eds, Advancements in Adaptive Optics*. Edited by Domenico B. Calia, Brent L. Ellerbroek, and Roberto Ragazzoni. *Proceedings of the SPIE*, Volume 5490, pp. 359-369 (2004). eXtreme Adaptive Optics Planet Imager: overview and status. pp 359–369
- Marois C., Doyon R., Nadeau D., Racine R., Riopel M., Vallée P., Lafrenière D., 2005, *PASP*, 117, 745
- Marois C., Lafrenière D., Doyon R., Macintosh B., Nadeau D., 2006, *ApJ*, 641, 556
- Marois C., Racine R., Doyon R., Lafrenière D., Nadeau D., 2004, *ApJL*, 615, L61
- Nielsen E. L., Close L. M., Guirado J. C., Biller B. A., Lenzen R., Brandner W., Hartung M., Lidman C., 2005, *Astronomische Nachrichten*, 326, 1033
- Racine R., Walker G. A. H., Nadeau D., Doyon R., Marois C., 1999, *PASP*, 111, 587
- Ren D., Wang H., 2006, *ApJ*, 640, 530
- Schreiber J., Thatte N., Eisenhauer F., Tecza M., Abuter R., Horrobin M., 2004, in *Ochsenbein F., Allen M. G., Egret D., eds, ASP Conf. Ser. 314: Astronomical Data Analysis Software and Systems (ADASS) XIII Data Reduction Software for the VLT Integral Field Spectrometer SPIFFI*. pp 380–+
- Soummer R., Aime C., Ferrari A., Sivaramakrishnan A., Oppenheimer B. R., Makidon R., Macintosh B., 2006, in *Aime C., Vakili F., eds, Direct Imaging of Exoplanets: Science & Techniques. Proceedings of the IAU Colloquium #200*, Edited by C. Aime and F. Vakili. Cambridge, UK: Cambridge University Press, 2006., pp.367-372 *Apodized Pupil Lyot Coronagraphs: Concepts and application to the Gemini Planet Imager*. pp 367–372
- Sparks W. B., Ford H. C., 2002, *ApJ*, 578, 543
- Tecza M., Eisenhauer F., Iserlohe C., Thatte N. A., Abuter R., Roehrl C., Schreiber J., 2003, in *Atad-Ettedgui E., D’Odorico S., eds, Specialized Optical Developments in Astronomy*. Edited by Atad-Ettedgui, Eli; D’Odorico, Sandro. *Proceedings of the SPIE*, Volume 4842, pp. 375-383 (2003). SPIFFI Image Slicer: High-Precision Optics at Cryogenic Temperatures. pp 375–383
- Tecza M., Thatte N. A., Eisenhauer F., Mengel S., Roehrl C., Bickert K., 2000, in *Iye M., Moorwood A. F., eds, Proc. SPIE Vol. 4008, p. 1344-1350, Optical and IR Telescope Instrumentation and Detectors*, Masanori Iye; Alan F. Moorwood; Eds. SPIFFI image slicer: revival of image slicing with plane mirrors. pp 1344–1350
- Thatte N. A., Tecza M., Eisenhauer F., Mengel S., Krabbe A., Pak S., Genzel R., Bonaccini D., Emsellem E., Rigaut F. J., Delabre B., Monnet G., 1998, in *Bonaccini D., Tyson R. K., eds, Proc. SPIE Vol. 3353, p. 704-715, Adaptive Optical System Technologies*, Domenico Bonaccini; Robert K. Tyson; Eds. SINFONI: a near-infrared AO-assisted integral field spectrometer for the VLT. pp 704–715
- Verinaud C., Hubin N., Kasper M., Antichi J., Baudoz P., Beuzit J.-L., Boccaletti A., Chalabaev A., Dohlen K., Fedrigo E., da Silva C. C., Feldt M., 2006, in *Aime C., Vakili F., eds, Direct Imaging of Exoplanets: Science & Techniques. Proceedings of the IAU Colloquium #200*, Edited by C. Aime and F. Vakili. Cambridge, UK: Cambridge University Press, 2006., pp.507-512 *The EPICS project: Exoplanets detection with OWL*. pp 507–512
- Vogelaar M. G. R., Terlouw J. P., 2001, in *Harnden Jr. F. R., Primini F. A., Payne H. E., eds, ASP Conf. Ser. 238: Astronomical Data Analysis Software and Systems X The Evolution of GIPSY—or the Survival of an Image Processing System*. pp 358–+